J|A|C|S
ARTICLES
Published on Web 03/08/2006

Kinetic Performance and Energy Profile in a Roller Coaster Electron Transfer Chain: A Study of Modified Tetraheme-Reaction Center Constructs

Jean Alric,[†] Jérôme Lavergne,*[,§] Fabrice Rappaport,[†] André Verméglio,[§] Katsumi Matsuura,[‡] Keizo Shimada,[‡] and Kenji V. P. Nagashima*[,‡]

Contribution from the Institut de Biologie Physico-Chimique, 13 rue Pierre et Marie Curie 75005 Paris, France, Department of Biology, Tokyo Metropolitan University, Minamiohsawa 1−1, Hachioji, Tokyo 192-0397, Japan, and CEA-Cadarache DSV-DEVM Laboratoire de Bioénergétique Cellulaire, UMR 6191 CNRS-CEA-Aix-Marseille II, F-13108 Saint Paul-lez-Durance Cedex, France

Received November 30, 2005; E-mail: jerome.lavergne@cea.fr; nagashima-kenji@c.metro-u.ac.jp

Abstract: In many electron-transfer proteins, the arrangement of cofactors implies a succession of uphill and downhill steps. The kinetic implications of such arrangements are examined in the present work, based on a study of chimeric photosynthetic reaction centers obtained by expressing the tetraheme subunit from *Blastochloris viridis* in another purple bacterium, *Rubrivivax gelatinosus*. Site-directed mutations of the environment of heme c_{559}, which is the immediate electron donor to the primary donor P, induced modifications of this heme's midpoint potential over a range of 400 mV. This resulted in shifts of the apparent midpoint potentials of the neighboring carriers, yielding estimates of the interactions between redox centers. At both extremities of the explored range, the energy profile of the electron-transfer chain presented an additional uphill step, either downstream or upstream from c_{559}. These modifications caused conspicuous changes of the electron-transfer rate across the tetraheme subunit, which became ∼100-fold slower in the mutants where the midpoint potential of c_{559} was lowest. A theoretical analysis of the kinetics is presented, predicting a displacement of the rate-limiting step when lowering the potential of c_{559}. A reasonable agreement with the data was obtained when combining this treatment with the rates predicted by electron transfer theory for the individual rate constants.

Introduction

Current research on electron transfer (ET) proteins has revealed that in many instances the energy profile for successive transfer steps is not a gradual descent but is more akin to a roller coaster course, offering a succession of uphill and downhill steps. This means that, in complexes where the ET pathway involves a sequence of more than two cofactors, the midpoint potentials (E_m) of these redox centers are often found in an alternance of high/low/high values. This counterintuitive arrangement was first established for the tetraheme of some photosynthetic reaction centers (RC), as described below in greater detail. It has ever since emerged as a frequently encountered pattern.[1] Particularly demonstrative cases are [NiFe]-hydrogenase[2] or fumarate reductase,[3] which exhibit chains of multiple iron−sulfur clusters in which neutral [3Fe-4S] centers are inserted between highly electronegative [4Fe-4S] clusters, introducing very endergonic ET steps.[4] Other well-documented examples are, e.g., nitrate reductase[5] and formate dehydrogenase.[6] In this paper, we examine the kinetic issues raised by this type of energy profile, based on the study of a series of genetically engineered tetraheme-reaction center constructs.

Photosynthetic electron transfer is initiated by a photochemical charge separation in the reaction center complex (RC). In purple bacteria, the primary electron donor P is a special pair of bacteriochlorophylls whose excited state (P*) is a strong reductant inducing rapid reduction of electron acceptors. The oxidized special pair (P^+) is then reduced by an electron donor in the periplasmic space. It is important to remove rapidly the oxidizing equivalent from P^+ for several reasons. First, the P^+ state is incompetent for further photochemical charge separation. In addition, this state is a target for charge recombination with reduced acceptors, a process that results in a decreased effective yield and is also likely of generating noxious species.

In many purple bacteria, the direct electron donor to P^+ is a tetraheme cytochrome *c* bound to the LM core proteins at the

[†] Institut de Biologie Physico-Chimique.
[‡] Department of Biology, Tokyo Metropolitan University.
[§] CEA-Cadarache DSV-DEVM Laboratoire de Bioénergétique Cellulaire, UMR 6191 CNRS-CEA-Aix-Marseille II.

(1) Page, C. C.; Moser, C. C.; Chen, X.; Dutton, P. L. *Nature* **1999**, *402*, 47−52.
(2) Volbeda, A.; Charon, M. H.; Piras, C.; Hatchikian, E. C.; Frey, M.; Fontecilla-Camps, J. C. *Nature* **1995**, *373*, 580−587.
(3) Haas, A. H.; Lancaster, C. R. *Biophys. J.* **2004**, *87*, 4298−4315.
(4) Rousset, M.; Montet, Y.; Guigliarelli, B.; Forget, N.; Asso, M.; Bertrand, P.; Fontecilla-Camps, J. C.; Hatchikian, E. C. *Proc. Natl. Acad. Sci. U.S.A.* **1998**, *95*, 11625−11630.
(5) Bertero, M. G.; Rothery, R. A.; Palak, M.; Hou, C.; Lim, D.; Blasco, F.; Weiner, J. H.; Strynadka, N. C. *Nat. Struct. Biol.* **2003**, *10*, 681−687.
(6) Jormakka, M.; Tornroth, S.; Byrne, B.; Iwata, S. *Science* **2002**, *295*, 1863−1868.

10.1021/ja058131t CCC: $33.50

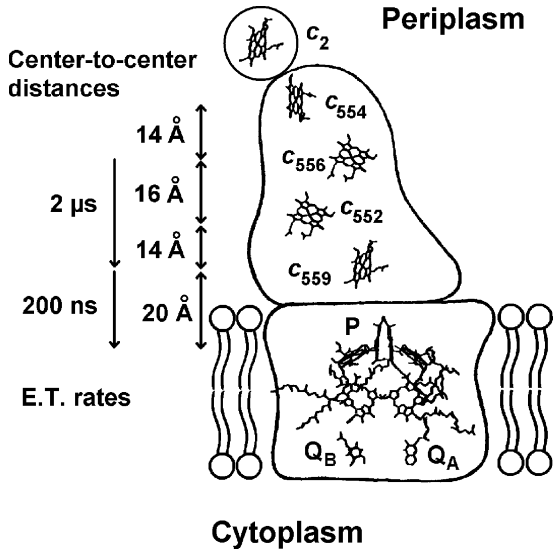

Figure 1. Scheme showing the arrangement of the cofactors in the RC of *B. viridis*.

periplasmic surface. The atomic structure of the reaction center complex of a purple bacterium, *Blastochloris viridis*, based on X-ray crystallography, showed that the arrangement of the four hemes in the cytochrome subunit is roughly linear and perpendicular to the membrane plane[7,8] The hemes have different properties in terms of absorption spectra and redox midpoint potentials.[9−13] Their arrangement is depicted by the scheme of Figure 1. The proximal heme to P (E_m = +500 mV) has the highest midpoint potential (+380 mV). Its α band peaks at 559 nm, hence its denomination as c_{559}. Moving away from P, the second heme, c_{552}, has a low midpoint potential, about +30 mV. The third heme, c_{556}, has again a high potential, about +320 mV. The fourth, most distal heme, c_{554}, has the lowest potential (−50 mV). It is the electron-transfer partner for the soluble electron donor, cytochrome c_2 (E_m = +300 mV) that shuttles electrons between the RC and the cytochrome bc_1 complex.[14,15] This means that all four hemes of the tetraheme subunit are active members of the electron-transfer pathway from cytochrome c_2 to P, in which two steps, from cytochrome c_2 to c_{554} and from c_{556} to c_{552}, are very uphill processes. Such a high-low-high-low arrangement of the hemes potentials appears to be a conserved feature in many species of purple bacteria and even in the distantly related green filamentous bacteria.[16] The reason such uphill electron-transfer steps are conserved, however, has not been clarified.

On the basis of the atomic structure of the *B. viridis* cytochrome subunit, charged amino acid residues near the hemes have been suggested to have strong effects on their electrostatic properties.[17,18] These residues are conserved even in species distantly related to *B. viridis*.[19] Evidence for the role of such charged residues was reported by Chen et al.,[20] who found that the replacement of an Arg by a Lys at position 264 in the *B. viridis* tetraheme lowered the E_m of c_{559} from +380 mV to +270 mV. In this mutant the rate of electron transfer from c_{556} to P^+ was nearly the same as in the wild type $(2\ \mu s)^{-1}$ although the reduction of P^+ by c_{559} was slightly faster $(105\ ns)^{-1}$ than that in the wild type $(190\ ns)^{-1}$. Further investigations, involving a broader range of changes of the electrostatic properties of the hemes are desirable to gain additional insight on the functional and evolutionary significance of the high-low-high-low E_m pattern. However, it has been difficult to make such mutants since the growth of *B. viridis* is very slow under nonphotosynthetic conditions.

Recently, it was shown that the *B. viridis* cytochrome subunit can be expressed in cells of the far-related purple bacterium *Rubrivivax gelatinosus* by engineering a gene replacement.[21] In this modified strain, the tetraheme is spontaneously assembled with the RC core subunits and works as the immediate electron donor to P^+. A further development was to construct a series of mutants with modified midpoint potentials of the hemes in the chimeric reaction center complex.[22] Since *R. gelatinosus* grows well under both photosynthetic and respiratory conditions, it becomes easier to obtain mutations impairing the photosynthetic activity. In this study, we focus on the kinetic consequences of modifications of the midpoint potential of heme c_{559}. We constructed chimeric reaction center complexes where the Arg202 of the cytochrome subunit was replaced by Glu (R202E), or the Arg264 was changed to Lys (R264K) and Leu (R264L). Strains carrying both mutations, R202E/R264K and R202E/R264L, were also constructed. This resulted in changes of the E_m values for c_{559} ranging from 420 to 0 mV. To interpret the effects on the kinetics of electron transfer across the multiheme chain, it was necessary to clarify the theoretical relationship between the observed kinetics and the rate constants for the individual reactions. The dependence of these step rate constants on the driving force can then be analyzed in the framework of current ET theory.

Experimental Section

Genetic Constructs. Mutants of *R. gelatinosus* in which the gene coding for the cytochrome subunit was removed were constructed for expressing the *B. viridis* cytochrome gene. This gene, in which nucleotides in focus were changed by a method of two-step PCR, was cloned into a suicide vector pJP5603 (Kmr) with the gene for the RC-M subunit of *R. gelatinosus*. After introduction of the plasmid into the *R. gelatinosus* mutant, cells resistant to kanamycin were selected. The incorporation of the mutated *B. viridis* cytochrome gene by homologous recombination was confirmed by PCR and DNA sequencing. All chimeric strains showed diminished growth rates with respect to WT *R. gelatinosus*, including the "native chimera" VC−F. This is probably

(7) Deisenhofer, J.; Epp, O.; Miki, K.; Huber, R.; Michel, H. *Nature* **1985**, *318*, 618−624.
(8) Deisenhofer, J.; Epp, O.; Sinning, I.; Michel, H. *J. Mol. Biol.* **1995**, *246*, 429−457.
(9) Alegria, G.; Dutton, P. L. *Biochim. Biophys. Acta* **1991**, *1057*, 258−1972.
(10) Alegria, G.; Dutton, P. L. *Biochim. Biophys. Acta* **1991**, *1057*, 239−1957.
(11) Dracheva, S. M.; Drachev, L. A.; Zaberezhnaya, S. M.; Konstantincv, A. A.; Semenov, A. Y.; Skulachev, V. P. *FEBS Lett.* **1986**, *205*, 41−46.
(12) Vermeglio, A.; Richaud, P.; Breton, J. *FEBS Lett.* **1989**, *243*, 259−263.
(13) Nitschke, W.; Rutherford, A. W. *Biochemistry* **1989**, *28*, 3161−3168.
(14) Garcia, D.; Richaud, P.; Verméglio, A. *Biochim. Biophys. Acta (BBA) − Bioenerg.* **1993**, *1144*, 295−301.
(15) Knaff, D. B.; Willie, A.; Long, J. E.; Kriauciunas, A.; Durham, B.; Millett, F. *Biochemistry* **1991**, *30*, 1303−1310.
(16) Nitschke, W.; Dracheva, S. M. In *Anoxygenic Photosynthetic Bacteria*; Blankenship, R. E., Madigan, M. T., Bauer, C. E., Eds. Kluwer Academic Publishers: Dordrecht, The Netherlands, 1995; pp 775−805.
(17) Voigt, P.; Knapp, E. W. *J. Biol. Chem.* **2003**, *278*, 51993−52001.
(18) Gunner, M. R.; Honig, B. *Proc. Natl. Acad. Sci. U.S.A.* **1991**, *88*, 9151−9155.
(19) Nagashima, K. V. P.; Sakuragi, Y.; Shimada, K.; Matsuura, K. *Photosynth. Res.* **1998**, *55*, 349−355.
(20) Chen, I. P.; Mathis, P.; Koepke, J.; Michel, H. *Biochemistry* **2000**, *39*, 3592−3602.
(21) Maki, H.; Matsuura, K.; Shimada, K.; Nagashima, K. V. *J. Biol. Chem.* **2003**, *278*, 3921−3928.
(22) Nagashima, K. V. P.; Alric, J.; Matsuura, K.; Shimada, K.; Verméglio, A. In *Photosynthesis: Fundamental Aspects to Global Perspectives*; van der Est, A., Bruce, D., Eds.; Allen Press: Montréal, Canada, 2005; pp 325−327.

Table 1. Compilation of Data for Redox Titrations and Kinetics on the Various Strains Examined Here

strains	E_m (mV) P	c_{559}	c_{552}	c_{556}	c_{554}	ET rates (s^{-1}) k^{obs}_{fast}	k^{obs}_{slow}	ref
B. viridis WT RC	+500	+380	+30	+310	−70	3.0×10^6	4.1×10^5	*a*
B. viridis R264K RC	+500	+270	+30	+310	−70	6.6×10^6	3.2×10^5	*a*
Native chimeric RC (VC−F)	+350	+420	+60	+310	−60	9.9×10^5	3.0×10^4	*b*
R202E chimeric RC	+400	+290	+65	+380	−30	1.1×10^6	2.7×10^4	*c*
R264K chimeric RC	+400	+280	+40	+360	−50	1.0×10^6	6.9×10^4	*c*
R264L chimeric RC	+415	0	+130	+330	−70	6.9×10^6	2.3×10^3	*c*
R264E chimeric RC	+400	0	+130	+320	−60	4.6×10^6	7.7×10^2	*c*
R202E/R264K chimeric RC	+380	+20	+150	+340	−30	6.3×10^6	4.3×10^4	*c*
R202E/R264L chimeric RC	+390	−10	+90	+330	−30	7.7×10^6	9.9×10^2	*c*

[a] Chen et al.[20] [b] Alric et al.[24] [c] This work.

due to the fact that the soluble reductant to the tetraheme is a high-potential iron−sulfur protein (HiPIP) in *R. gelatinosus*, whereas it is cytochrome c_2 in *B. viridis*, so that the chimeric tetraheme has to interact with a nonphysiological partner. The VC−F growth rate was thus ∼27% that of the WT. The mutations affecting the c_{559} heme caused a further halving of the growth rate. All strains were however able to grow photosynthetically.

Redox Titrations. Cells of the *R. gelatinosus* mutants were grown photosynthetically under anaerobic conditions and disrupted by one passage through a French pressure cell. Membranes were collected by differential ultra-centrifugations and suspended in a buffer containing 50 mM potassium phosphate (pH 7.0). Redox titrations of the *c*-type hemes and of the primary donor P were carried out as described previously.[21]

Flash-Induced Kinetics. Electron-transfer kinetics in the mutated chimeric RC were investigated using a laboratory-built spectrophotometer, where the measuring beam consist of discrete monochromatic pulses of a few nanoseconds duration from an optical parametric oscillator (OPO) laser.[23] The redox changes of P were monitored from the associated absorption changes at 605 nm using membrane preparations poised (unless mentioned otherwise) around a redox potential of 200 mV by addition of 100 μM sodium ascorbate and 10 μM diamino durene (DAD).

Mathematical Calculations. The calculation (symbolic/numerical) of the eigenvalues of the kinetic matrixes was handled using Mathcad (Matsoft Inc.).

Results

Redox Titrations. To modify the midpoint potential of heme c_{559}, the two positively charged residues Arg 202 and Arg 264 located in the vicinity of this heme appeared as good targets for site-directed mutagenesis. It was previously noted,[17,18] that these basic residues should contribute to the neutralization of the heme's propionic acids, and thus raise the midpoint potential of c_{559}. Their replacement, especially by the negatively charged glutamates in mutants R202E and R264E is thus expected to decrease this potential. Table 1 indicates the results of redox titrations carried out in membranes of the various strains, by recording the absorption spectra in the α band region of the hemes and in the Q_x band of P as a function of the ambient potential.

As previously discussed,[24] the titration of the P^+/P couple in the VC−F strain did not come out as a simple Nernst curve, but showed a major wave around 350 mV and a smaller one around 400 mV. In the other chimeric strains (as well as in *R. gelatinosus* WT) only the 400 mV wave was present. Strain VC−F differs from the other cases because the midpoint potential of heme c_{559} is higher than that of P, allowing the (partial) titration of the latter in the presence of the reduced neighboring heme, at variance with the standard situation. The split titration and the comparison with the other strains are indicative of a ∼50 meV electrostatic interaction between P and c_{559}. The interplay between electrostatic interactions, redox titration data and the energy landscape is a general concern in the present work and will be addressed in detail in the next section.

As shown in Table 1, the largest effect on the $E_m(c_{559})$ in the single mutants was obtained with R264L or R264E, where the potential was decreased by 420 mV compared with the VC−F strain (chimera with the native tetraheme of *B. viridis*). The decrease was similar in the double mutants, failing to fulfill the expectation of a cumulative effect. The mutations did not affect significantly the E_m of P (taking into account the 50 mV interaction effect). The position of the α peak of "c_{559}" was affected by the mutations, shifting toward shorter wavelengths as the E_m was decreased. It remained at 559 nm in VC−F and R202E, but decreased to ∼556 nm in R264K (as previously observed in the homologous *B. viridis* mutant[20]). In the R264L/E and double mutant strains the peak was around 552−553 nm and there was thus some ambiguity with these strains for ascribing the low potential redox titration waves to hemes "c_{559}" and c_{552}. This ambiguity was dispelled on the following grounds. First, the choice adopted in Table 1 leaves almost unchanged the true E_m of c_{552} — when properly taking into account the interaction between c_{559} and c_{552}. Indeed, for the bottom four strains in Table 1, the average E_m ascribed to c_{552} (125 mV) is 70 mV higher than the average value for the three other chimeric strains. This upward shift is expected to occur when c_{552} is titrated in the presence of the oxidized c_{559} at variance with the standard situation. Its magnitude is close to that (77 meV) estimated for the interaction between c_{559} and c_{552} in the electrostatic calculations reported in ref 18. The other option ($E_m(c_{559}) \approx +130$, $E_m(c_{552}) \approx 0$) would require an unlikely systematic shift of c_{552} by about −55 mV. Additional arguments are provided by the kinetic study described later: for these strains the observed rates are consistent with the option $E_m(c_{559}) < E_m(c_{552})$ but not with the alternative one; also, the fast phase

(23) Béal, D.; Rappaport, F.; Joliot, P. *Rev. Sci. Instr.* **1999**, *70*, 202−207.
(24) Alric, J.; Cuni, A.; Maki, H.; Nagashima, K. V.; Verméglio, A.; Rappaport, F. *J. Biol. Chem.* **2004**, *279*, 47849−47855.

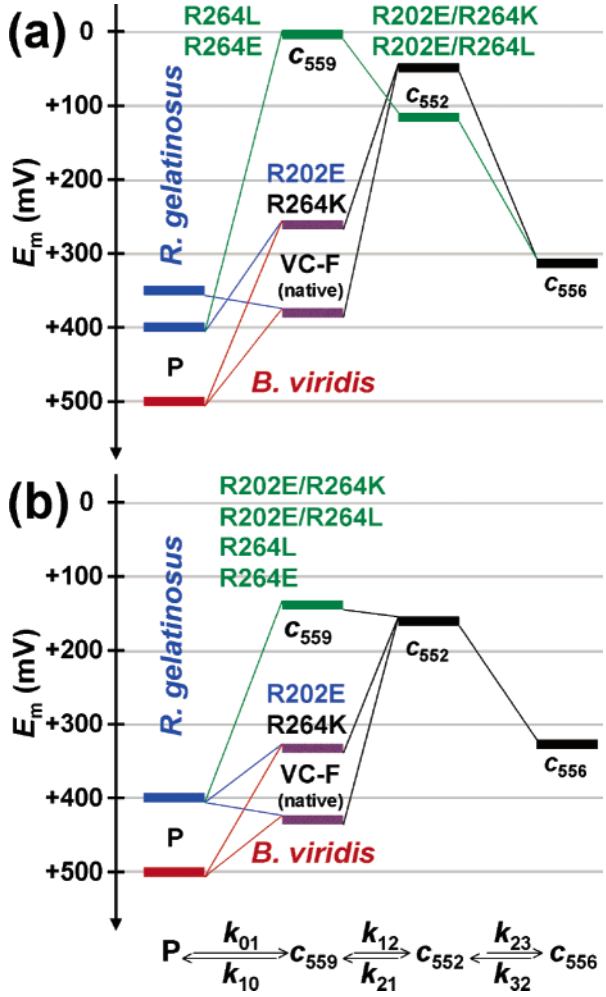

Figure 2. Energy profile of the donor chain in the various strains investigated in this study. (a) Experimentally obtained midpoint potentials (Table 1). (b) Energy profiles corrected from electrostatic interactions between redox centers: the E_m of each center is given in the presence of the other centers in their oxidized state.

reflecting the direct reduction of P^+ by c_{559} titrates in around 0 mV.

Figure 2a gives an overview of the energetic pattern in the various strains, as it appears from the midpoint potentials of Table 1. This scheme, however, does not properly take into account the interactions between the various redox carriers, which modify the energy profile depending on the distribution of oxidized/reduced species. This issue is examined in detail below.

Interactions and Energy Landscape. In general, if the electrostatic interaction between two redox centers A and B is Ψ_{AB} (> 0) (expressing energies in eV), the ΔG pertaining to the electron transfer between them is as follows:

$$\Delta G_{AB} = E_m^A - E_m^B + \Psi_{AB} \qquad (1)$$

E_m^A and E_m^B are the experimental midpoint potentials; the reaction is assumed to be exergonic from A to B ($E_m^A < E_m^B$), with ΔG negative (when $E_m^A > E_m^B$, Ψ_{AB} must be subtracted rather than added). In addition to this correction, one must include the possible shifts of E_m^A and E_m^B due to modifications of the redox states of neighboring carriers (other than A and B) with respect to the titration conditions. In Table 2, we have summarized the results of this procedure for the five different cases encountered here with respect to the ranking of midpoint potentials, as indicated in the first column. In this Table and in the following we ascribe subscripts 0 to 3 to P, c_{559}, c_{552}, and c_{556}, respectively. Thus, E_0 stands for E_m(P), etc. and (positive) interaction energies between redox centers i and j are denoted as Ψ_{ij}. To illustrate the procedure used for generating the expressions shown in Table 2, let us for example consider ΔG_{21} for the last row, when a single electron is present in the donor chain. Equation 1 is applied, with a minus sign for Ψ_{21} (uphill reaction), noting the following: (i) c_{552} is here, at variance with the titration situation, in the presence of the oxidized c_{556} and P so that it features as ($E_2 + \Psi_{32} + \Psi_{20}$); and (ii) c_{559} is in the presence of the oxidized c_{556} and P so that it features as ($E_1 + \Psi_{31} + \Psi_{10}$).

A simplifying assumption in the above treatment is that the separation between the E_m levels is large enough (e.g., >60 mV) so that the titration waves can be ascribed to individual redox centers. This is true in most cases, except for the high potential waves in VC−F, where, as previously discussed, the 70 mV difference between the E_m's of P and of c_{559} (Table 1) includes a $\Psi_{10} = 50$ mV interaction term. The true gap is thus only ∼20 mV and the two redox centers are expected to contribute to both titration waves with different weights (e.g., ∼2/3 of P, 1/3 of c_{559} in the 350 mV wave).

The interaction energies used in Table 2 are either derived from experimental data in the case of Ψ_{10} (in ref 24) and Ψ_{21} (this work), or estimated from electrostatic calculations.[18] We noticed above that the value of $\Psi_{21} \approx 70$ meV deduced from the shift of E_2 when c_{559} becomes more reducing than c_{552} is slightly lower than Gunner's estimate of 77 meV. Whether estimated from experiments or calculations, these interactions are consistent with an "effective" dielectric constant (or "screening factor"[25]) of about 14 for all nearest neighbor interactions (taking into account the center-center distances).

Figure 2b shows the energy profile after correcting for the interactions as described above. The E_m of each redox center is indicated in the presence of all other centers in their oxidized state (i.e., the ΔG's are those for the single electron case in Table 2). An important consequence of these corrections is that the height of the uphill step ΔG_{32} is markedly decreased (by ∼115 meV) with respect to the estimate obtained directly from titration values (e.g., the corrected ΔG_{32} for *B. viridis* is 165 meV rather than 280 meV). One should also notice that these effects have the consequence of magnifying the apparent changes of $E_m(c_{559})$ caused by the mutations. The observed range extends from 420 mV in VC−F to ∼0 mV for the four last strains listed in Table 1. However, in the first case, c_{559} is the highest potential species, titrated in the presence of all other centers in their oxidized state. The situation is reversed for the low potential mutants, where c_{559} is titrated in the presence of all other centers in their reduced state. Thus, from the apparent span of 420 mV, one must subtract $\Psi_{10} + \Psi_{21} + \Psi_{31} = 134$ meV and the true effect of the mutations is to downshift $E_m(c_{559})$ by ∼286 mV.

Kinetics. We will now focus on the kinetic results obtained with membranes from these various strains, when monitoring the reduction of the photooxidized primary donor P^+. These kinetics were analyzed in terms of two exponential phases (fast

(25) Schutz, C. N.; Warshel, A. *Proteins* **2001**, *44*, 400−417.

Table 2. Calculation of the ΔGs for the Three ET Steps, Incorporating the Corrections Due to Electrostatic Interactions[a]

strain	ΔG_{10}	ΔG_{21}	ΔG_{32}
B. viridis WT P > c_{559} > c_{556} > c_{552}	$E_1 - E_0 + \Psi_{10} - \Psi_{31}$ (†) −84 meV	$E_2 - E_1 + \Psi_{32} + \Psi_{21}$ (‡) −228 meV	$E_3 - E_2 - \Psi_{32} - \Psi_{21} + \Psi_{31}$ (‡) 172 meV
B. viridis R264K P > c_{556} > c_{559} > c_{552}	$E_1 - E_0 + \Psi_{10}$ (†) −180 meV	$E_2 - E_1 + \Psi_{21} + \Psi_{32} - \Psi_{31}$ (‡) −132 meV	$E_3 - E_2 - \Psi_{32} - \Psi_{21}$ (‡) 158 meV
VC−F c_{559} > P > c_{556} > c_{552}	$E_1 - E_0 - \Psi_{10} - \Psi_{31}$ (†) 6 meV	$E_2 - E_1 + \Psi_{21} + \Psi_{32} + \Psi_{10}$ (‡) −188 meV	$E_3 - E_2 - \Psi_{32} + \Psi_{31} - \Psi_{21}$ (‡) 142 meV $E_3 - E_2 - \Psi_{32} + \Psi_{31} - \Psi_{21} - \Psi_{20}$ (§) 128 meV
R202E R264K P > c_{556} > c_{559} > c_{552}	$E_1 - E_0 + \Psi_{10}$ (†) −60 meV; −70 meV $E_1 - E_0 + \Psi_{10} + \Psi_{31}$ (¶) −46 meV; −56 meV	$E_2 - E_1 + \Psi_{21} + \Psi_{32} - \Psi_{31}$ (‡) −117 meV; −132 meV $E_2 - E_1 + \Psi_{21} + \Psi_{32} + \Psi_{20} - \Psi_{31} - \Psi_{10}$ (¶) −153 meV; −168 meV	$E_3 - E_2 - \Psi_{32} - \Psi_{21}$ (‡) 193 meV; 198 meV $E_3 - E_2 - \Psi_{32} - \Psi_{21} - \Psi_{20}$ (¶) 179 meV; 184 meV
R264L R264E R202E/R264K R202E/R264L P > c_{556} > c_{552} > c_{559}	$E_1 - E_0 + \Psi_{10} + \Psi_{21}$ (†) −295 meV; −280 meV −240 meV; −280 meV $E_1 - E_0 + \Psi_{10} + \Psi_{21} + \Psi_{31}$ (¶) −281 meV; −266 meV; −226 meV; −266 meV	$E_2 - E_1 - \Psi_{21} + \Psi_{20} - \Psi_{10}$ (†) 24 meV; 24 meV; 24 meV; −6 meV $E_2 - E_1 - \Psi_{21} + \Psi_{32} + \Psi_{20} - \Psi_{31} - \Psi_{10}$(¶) 62 meV; 62 meV; 62 meV; 32 meV	$E_3 - E_2 - \Psi_{32} - \Psi_{20}$ (¶) 134 meV; 124 meV; 124 meV; 174 meV;

[a] The E_m values are the measured midpoint potentials (Table 1), with subscript $n = 0$ to 3 standing for P, c_{559}, c_{552}, and c_{556}, respectively. The interaction energies are $\Psi_{10} = 50$ meV (24), $\Psi_{21} = 70$ meV (this work), $\Psi_{32} = 52$ meV, $\Psi_{31} = 14$ meV (18) and $\Psi_{20} = 14$ meV (assumed). The five cases considered (rows) depend on the ranking of the midpoint potentials, as indicated in the first column. Subcases (retaining those which are experimentally relevant) are also considered depending whether one or two electrons are present in the system (following P photooxidation), as specified: (†) Two electrons, including one in c_{556}; (‡) Two electrons, including one in P; (§) Two electrons, including one in c_{559}; (¶) One electron.

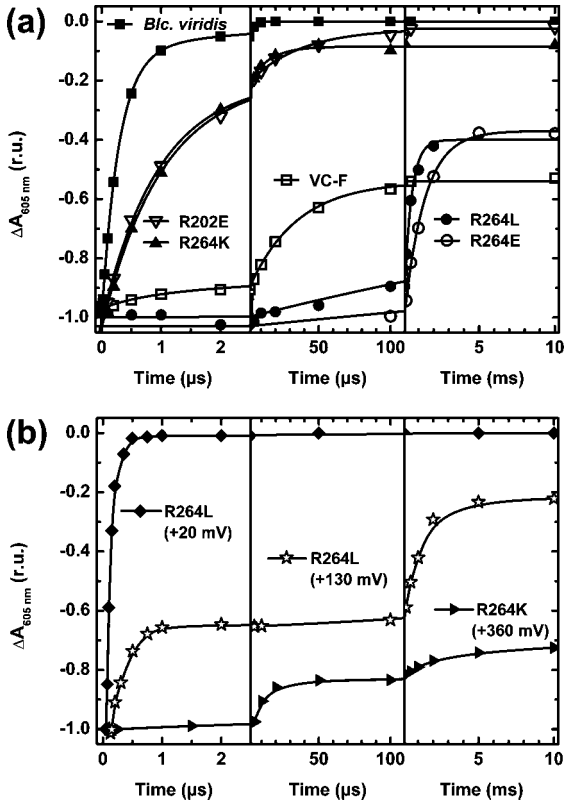

Figure 3. Kinetics of P^+ reduction following a single laser flash in membranes of the various strains, as indicated. The lines are fits by a sum of two exponential components. (a) The redox potential was poised around +200 mV by a DAD/ascorbate mixture. (b) Traces obtained at different values of the redox potential, as indicated.

and slow), as discussed below. The corresponding rate constants have been compiled in Table 1, with (part of) the kinetic traces shown in Figure 3. The results shown in panel (a) were obtained in the presence of ascorbate and diamino durene (DAD), poising the ambient redox potential around 200 mV. Thus, the low potential hemes c_{552} and c_{554} are essentially oxidized in the dark-adapted state, heme c_{556} is reduced and c_{559} will be oxidized in R264L and R264E and in the double mutants, reduced in the other strains. In the latter case, a fast reduction phase of P^+ is expected, reflecting the relaxation of the c_{559} $P^+ \leftrightarrow c_{559}^+$ P equilibrium. Electron transfer from the distal heme c_{556} (involving the uphill step across heme c_{552}) will then reduce c_{559}. This may be accompanied by a slow phase of P^+ reduction if the equilibrium constant with c_{559} is such that the reduction of P^+ was not completed during the first phase. In the case where c_{559} is initially oxidized (R264L/E and double mutants), the reduction of P^+ will entirely proceed through the second process involving the electron originating from c_{556}. To obtain the rate of the electron transfer from the proximal heme to P in these membranes, we made additional measurements, as illustrated in panel (b), poising the ambient potential around 20 mV, to ensure partial reduction of c_{559}. This restored a fast phase as expected, with $t_{1/2} \approx 100$ ns (k_{fast} indicated in Table 1). At intermediate potentials (∼130 mV), a fast phase of smaller amplitude and 2−3-fold slower rate was observed. This intermediary phase, attributed to the transfer from c_{552} to P^+, is consistent with the attribution of the midpoint potentials of 0 mV and +130 mV to hemes c_{559} and c_{552}, respectively. We also ran experiments with R264K and R202E at a higher potential (360 mV), which resulted in a mixed population of initial states including a significant fraction of the (c_{556} c_{559}^+ P) state and a negligible amount of reduced c_{559}. Accordingly, the fast phase was suppressed, while the rate of the slow phase was similar to that found in the traces of Figure 3a. The results concerning the WT and R264K mutant of *B. viridis* in Table 1 are those of references 20 and 26. Our own kinetic data for the *B. viridis* WT agree with these data. In particular, the rate of the slow phase, which has a small amplitude in this material, matches that determined by Ortega and Mathis[26] for the ET from c_{556} to c_{559}, by recording the absorption changes of the hemes.

The shift of E_1 toward lower potentials in the family of chimeric reaction centers results in a ∼6-fold acceleration of

(26) Ortega, J. M.; Mathis, P. *Biochemistry* **1993**, *32*, 1141−1151.

the fast phase and a ~100-fold slowing down of the slow phase. To discuss these results, we need to clarify the connection between the rate constants for the individual ET steps (the k_{ij} featuring in the scheme of Figure 2) and the observed rates k_{fast} and k_{slow}. However, before dealing with this issue, it is important to note, as explained below, that the observed kinetics lead to some modification of the energetic picture derived from redox titrations.

Dynamic Equilibria. When examining the kinetics of Figure 3 in relation to the energetic data of Tables 1 and 2, some systematic mismatches appear, concerning the extents of the two kinetic phases. Considering first the extent of the fast phase, the values of ΔG_{10} featured in Table 2 would predict about 50% for VC−F and 94−91% for R202E and R264K, whereas the observed values are ~5 and 80%, respectively. This suggests that the effective ΔG_{10} controlling the ET relaxation after the flash is significantly larger than indicated by the titrations. Another discrepancy between the titration data and the kinetic data concerns the final levels (≥ 5 ms) reached for VC−F, R264L, and R264E, which still involves ~50% oxidized P. This should reflect essentially the ET equilibrium between the distal high potential heme c_{556} and P. In the case of VC−F, two electrons are present in the chain after the flash, initially located in c_{556} and c_{559}. As noticed above, the small extent of the fast phase implies that c_{559} is significantly more electropositive than P so that one electron is expected to remain trapped on this heme, while the other one equilibrates between c_{556} and P. In the case of the R264L/E strains, we are dealing with a single electron (initially in c_{556}) and c_{559} is too electronegative (as well as c_{552}) to be reduced to a significant extent at equilibrium. Therefore, the final (≥5 ms) levels of P^+ shown in Figure 3 imply that the equilibrium constant between c_{556} and P is close to 1. Again, this differs significantly from the estimate derived from redox titrations where $\Delta G_{30} = E_3 - E_0$ (no interaction correction is required here) is −40 meV for VC−F or −55 meV for the other strains, implying an equilibrium constant of 5−9 (i.e., a final level with 80−90% reduced P). Taken together, the requirements for raising ΔG_{10} (extent of the fast phase) and ΔG_{30} (final equilibrium) suggest that the midpoint potential of P (E_0) is mainly responsible for the discrepancy and that its effective value during the kinetics is more negative by at least 40 mV than the titration value. Two effects may be expected to contribute to this shift: the interaction with the semiquinone (Q_A^- at short times, Q_B^- in the ms-range) on the acceptor side[27] and the effect of the delocalized membrane potential generated by charge separation.[28,29]

Step Rate Constants vs. Energy Profile. When varying the midpoint potential of the c_{559} heme (E_1), the driving forces for two ET steps are modified, i.e., ΔG_{10} and ΔG_{21}, which will affect the corresponding rate constants (k_{10}, k_{01}, k_{21}, k_{12}). ET theory predicts a parabolic dependence of ln(k) on the driving force. An empirical formula has been proposed by Moser and Dutton,[30] which was shown to account with reasonable accuracy for a wealth of experimental data and has the advantage of featuring only one adjustable parameter (the reorganization energy λ). The expression reads as follows:

$$\log k_{downhill} = 15 - 0.6R - 3.1\frac{(\Delta G + \lambda)^2}{\lambda} \qquad (2)$$

where R is the edge-to-edge distance (in Å) and ΔG the driving force (in eV) between electron donor and acceptor (ΔG is negative for a downhill reaction). For endergonic reactions (uphill ET), the rate constant is obtained by applying a Boltzmann factor to the downhill expression 2:

$$k_{uphill} = k_{downhill} \exp\left(\frac{\Delta G}{RT}\right) \qquad (3)$$

The factor 3.1 for the quadratic term in eq 3 is not the log(e)/4 $k_BT \approx 4.3$ term expected for the semiclassical Marcus' equation,[31] but somewhat smaller to fit the expressions derived when incorporating nuclear tunneling. This is responsible for the need to add a second equation (eq 3) to deal with uphill transfer and for the discontinuous slope when crossing the $\Delta G = 0$ value (see Figures 4−5). This problem does not arise in the Marcus equation, nor in the fully quantum mechanical equation of Bixon and Jortner,[32] where the Boltzmann relationship is obtained by just changing the sign of ΔG. Nevertheless, despite its tinkered look, the distortion implied by the approximate formula remains acceptable.

We can use the above equations to obtain an approximate picture for the dependence on E_1 of the step rate constants in the various systems that we investigated. This is shown in Figure 4 for *B. viridis* and in Figure 5 for the chimeric constructs. We first focus on the case of the *B. viridis* RC that will provide a general framework for discussing the relationship between the "step rate constants" k_{ij} and the observed kinetics for P^+ reduction. Figure 4a gives an overall view of the ln(k_{ij}) dependence on E_1. The edge-to-edge distances were taken from the crystallographic structure of *B. viridis*:[7,8] $R_{10} = 12.3$ Å, $R_{21} = 6.97$ Å, and $R_{32} = 7.89$ Å. The values of E_2 and E_3 are those of *B. viridis* corrected for a one-electron configuration. The value of E_0 was further shifted by −40 meV, assuming that the conclusions of the previous section also apply to *B. viridis*. The values of λ were estimated to fit the experimental data, as explained below. The rate constants k_{32} and k_{23} do not depend on E_1 and feature as horizontal lines. The other curves are parabolic with vertical locations governed by the ET distances: the shorter distance between c_{552} and c_{559} (R_{21}) than between c_{559} and P (R_{10}) results in a vertical offset by 3 decades.

Kinetics: Analytical Treatment and Approximations. We now discuss the relation between the step rate constants and the effective rates obtained for the two phases of P^+ reduction. The differential equations corresponding to the kinetic scheme of Figure 2 can be solved analytically. One state of the ET chain is specified by the distribution of "electrons" (reduced centers) over the four redox centers. We are interested in the relaxation kinetics following the photooxidation of P, during which the number of electrons present in each chain remains constant. One can thus deal separately with the families of states with 1, 2, and 3 electrons. Then, considering for instance the 4 configura-

(27) Ginet, N.; Lavergne, J. *Biochemistry* **2000**, *39*, 16252−16262.
(28) Dracheva, S. M.; Drachev, L. A.; Konstantinov, A. A.; Semenov, A.; Skulachev, V. P.; Arutjunjan, A. M.; Shuvalov, V. A.; Zaberezhnaya, S. M. *Eur. J. Biochem.* **1988**, *171*, 253−264.
(29) Rappaport, F.; Béal, D.; Verméglio, A.; Joliot, P. *Photosynthesis Research* **1998**, *55*, 317−323.
(30) Moser, C. C.; Dutton, P. L. *Biochim. Biophys. Acta* **1992**, *1101*, 171−176.
(31) Marcus, R. A.; Sutin, N. *Biochim. Biophys. Acta (BBA) − Rev. Bioenerg.* **1985**, *811*, 265−322.
(32) Bixon, M.; Jortner, J. *FEBS Lett.* **1986**, *200*, 303−308.
(33) Shopes, R. J.; Levine, L. M. A.; Holten, D.; Wraight, C. A. *Photosynth. Res.* **1987**, *12*, 165−180.

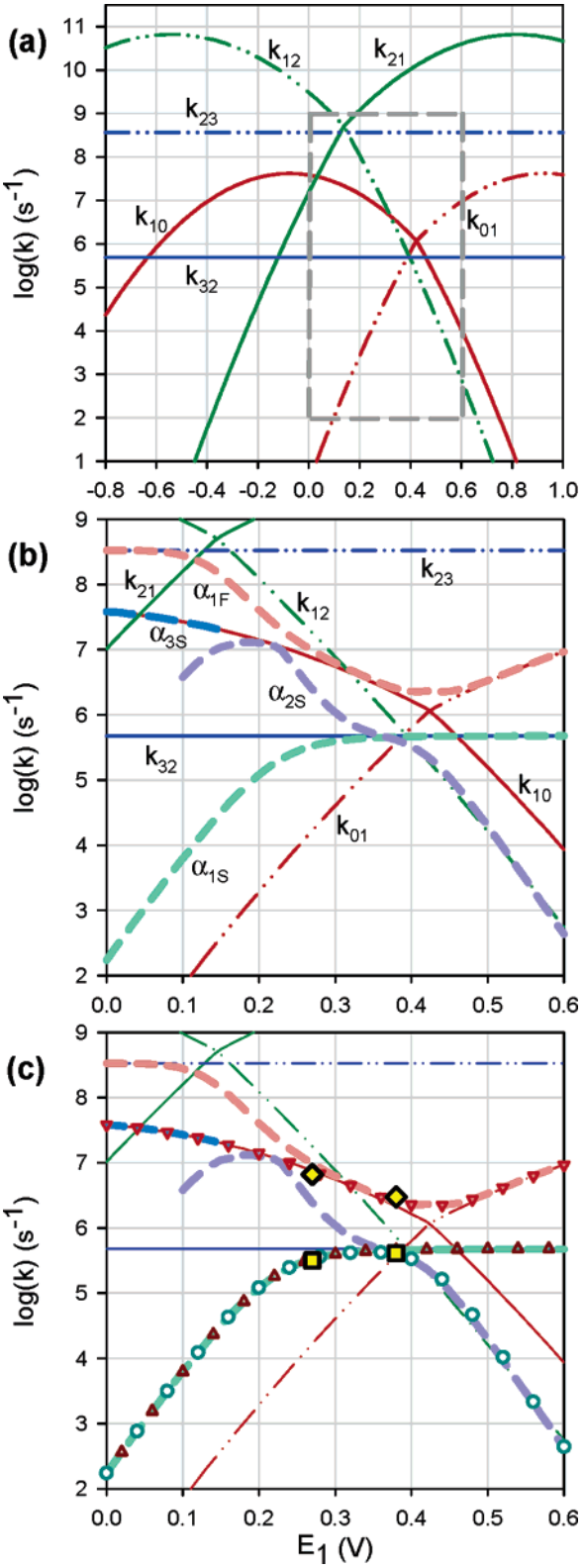

Figure 4. Step rate constants and rates of the fast and slow phases in the donor chain of *B. viridis*, when varying the midpoint potential of heme c_{559} (E_1). (a) Step rate constants computed with eqs 2−3, using parameters described in the text. The gray square indicates the region shown in panels b and c. (b) Same as a, with, in addition, the relevant eigenvalues (thick dashed lines) controlling the fast and slow phases of P^+ reduction, as discussed in the text. (c) Same as b, with, in addition, the plots for the approximation functions given by eq 6 (red triangles), eq 9 (brown triangles) and eq 12 (cyan circles). The yellow symbols are the experimental values from Table 1 for k_{fast} (diamonds) and k_{slow} (squares). They correspond from right to left to *B. viridis* WT and mutant R264K.

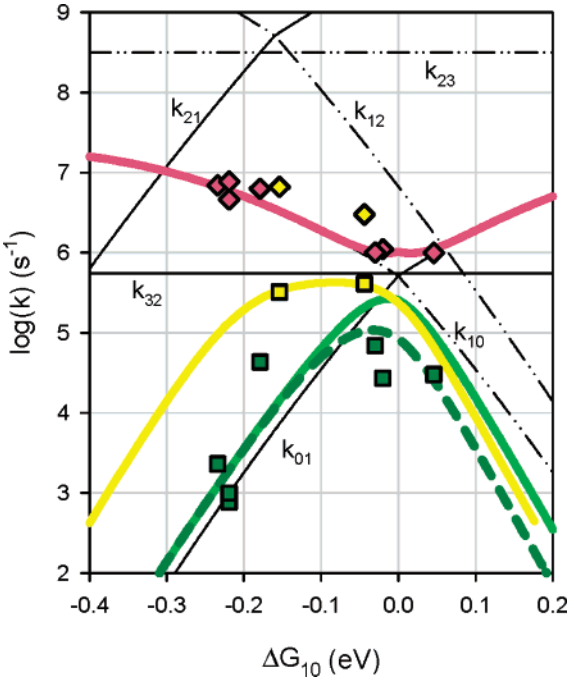

Figure 5. Step rate constants and rates of the fast and slow phases in the donor chain of the chimeric strains, when varying the midpoint potential of heme c_{559}. The step rate constants computed from eqs 2−3, using parameters described in the text, are shown as thin black lines. The thick solid lines are plots of the approximation formulas for k_{fast} (eq 6; pink) and k_{slow} (eq 12; green). The dashed green line is also a plot of eq 12, using modified parameters (see text). The yellow line is the corresponding curve for the *B. viridis* parameters (featuring as cyan circles in Figure 4c). The symbols show the experimental data for the fast (diamonds) and slow (squares) phases: pink and green for the chimeric strains, yellow for *B. viridis*. For the chimeric strains, the symbols correspond, from right to left, to strains: VC−F, R202E, R264K, R202E/R264K, R264E, R202E/R264L, and R264L. The horizontal scale in this figure is ΔG_{10} rather than E_1 (as in Figure 4), allowing a comparison between the data from *B. viridis* and from the chimeras (it also minimizes representation problems raised by the effects of interactions discussed about Table 2).

tions with a single electron, the state of the system can be described by a vector $\mathbf{S_1}$, where the successive rows indicate the fractions of the various states (see Appendix A in the Supporting Information).

The evolution of $\mathbf{S_1}(t)$ is obtained by solving a system of ordinary differential equations that can be written as follows

$$\frac{d\mathbf{S_1}(t)}{dt} = \mathbf{M_1}\mathbf{S_1}(t) \tag{4}$$

where $\mathbf{M_1}$ is a matrix incorporating the k_{ij}.

The solution of eq 4 is a sum of exponential components

$$\mathbf{S_1}(t) = \sum_{i=1}^{4} C_i \mathbf{V}_i e^{\alpha}{}_i t \tag{5}$$

The α_i's are the eigenvalues of the matrix $\mathbf{M_1}$ and the $\mathbf{V}_i$'s are the corresponding eigenvectors. The scalar constants C_i are chosen for matching the imposed initial condition on $\mathbf{S_1}(0)$. One of the four eigenvalues equals 0, corresponding to the final equilibrium state when the relaxation is complete. The same procedure can be applied to the families of states with two (6 states) or three electrons (4 states), constructing the transformation matrixes $\mathbf{M_2}$ or $\mathbf{M_3}$ (see Appendix A in the Supporting Information).

The analytical expressions for the nonzero eigenvalues of the **M** matrixes are quite complicated, but they can be readily computed numerically by a mathematical software. The relevant eigenvalues obtained in this manner were plotted in Figures 4b and c (thick dashed lines). They are labeled α_{1S}, α_{2S}, and α_{3S}, meaning the smallest nonzero eigenvalues (with inverted sign) of $\mathbf{M_1}$, $\mathbf{M_2}$, and $\mathbf{M_3}$, respectively, and α_{1F} for the next eigenvalue of $\mathbf{M_1}$ (the corresponding eigenvalue α_{2F} of $\mathbf{M_2}$ is very close to α_{1F} almost everywhere and was not plotted for clarity). Only a section of α_{3S} is shown: it is close to k_{10} everywhere. To gain a more intuitive grasp of the significance of these eigenvalues, it would be desirable to obtain simpler approximate formulas. We will now derive such formulas and check their adequacy against the "true" rates obtained from eigenvalues.

The fast phase concerns the relaxation of the ET equilibrium between heme c_{559} and P and one expects its rate to be close to

$$k_{\text{fast}}^{ap} = k_{10} + k_{01} \tag{6}$$

For the rate of the slow phase, assuming that a single electron is present, we apply a steady-state approximation as described in Appendix B in the Supporting Information. For the effective forward rate constant from c_{556} to P, we obtain (eq S14)

$$k_{30} = \left(\frac{1}{k_{32}} + \frac{1}{K_{32}k_{21}} + \frac{1}{K_{31}k_{10}}\right)^{-1} \tag{7}$$

where the K's are the equilibrium constants

$$K_{32} = \frac{k_{32}}{k_{23}} = \exp\left(-\frac{\Delta G_{32}}{z}\right)$$

$$K_{31} = \frac{k_{32}k_{21}}{k_{23}k_{12}} = \exp\left(-\frac{\Delta G_{31}}{z}\right) \tag{8}$$

with $z = RT$ in Faraday-V (R is the gas constant and T the temperature). The relaxation rate is the sum of the forward and backward rate constants (the latter cannot be neglected since the overall equilibrium constant K_{30} is close to 1 in the chimeric strains). Thus, the approximation formula searched for the slow phase is as follows

$$k_{\text{slow}}^{ap} = k_{30} + k_{03} = k_{30}\left(1 + \frac{1}{K_{30}}\right) \tag{9}$$

The approximation formulas for the fast and slow phases of P^+ reduction were plotted in Figure 4c for comparison with the eigenvalues. The open red triangles are a plot of k_{fast}^{ap} according to eq 6. It is very close to the eigenvalue (α_{1F} or α_{2F}) for $E_1 >$ 0.25 V. At lower E_1, the uphill "backward" rate constant k_{12} becomes larger than k_{10}, because of the smaller distance between c_{559} and c_{552}. Thus, an electron starting from c_{559} is increasingly taken up by c_{552}, which accelerates the fast reduction phase of P^+, while decreasing its amplitude. In the low range of E_1 values, it is necessary to fully reduce the donor chain to isolate kinetically the ET from c_{559} to P (as mentioned above, the values of "k_{fast}" in Table 1 were obtained in ad hoc experiments at low ambient potential) and α_{3S} becomes the relevant eigenvalue in this respect. Thus, the formula of eq 6 is always an excellent approximation for the experimental k_{fast}.

The open brown triangles in panel c are a plot of $k_{\text{slow}}{}^{ap}$ (eq 9). It is superimposed on the eigenvalue α_{1S}. Both functions appear parallel to k_{01} in the low range of E_1 and level off when reaching k_{32}. The reason for this appears when examining eq 7. If one of the three terms in this equation predominates over the others, then this implies a definite rate-limitation regime (for a more detailed discussion, see Appendix B, Supporting Information). For instance, if $1/k_{32}$ predominates, this means that the limiting step is $c_{556} \rightarrow c_{552}$; if the second or third term predominates, the limitation bears on the second or last ET step. Notice that products such as $K_{32}k_{21}$ (second term) or $K_{31}k_{10}$ (third term) express the electronic current in the $c_{552} \rightarrow c_{559}$ or $c_{559} \rightarrow$ P reaction, respectively, when upstream equilibrium is satisfied, which is precisely the definition of a rate-limiting step. If, for instance the limiting step is the reaction $c_{559} \rightarrow$ P, this does not necessarily mean that k_{10} is small compared with k_{32} and k_{21}, but may as well be due to the smallness of K_{31} (resulting in a small amount of reduced c_{559} throughout the process). As illustrated below, this effect actually predominates when E_1 is displaced toward low potentials, because the decrease of K_{31} (height of the upstream barrier) prevails on the increase of k_{10}, which, according to ET theory levels off when $-\Delta G_{10}$ approaches λ and decreases beyond this value. Looking at the rate constants featured in Figure 4, the first term $1/k_{32}$ predominates for $E_1 > 0.3$ V and the third term $1/(K_{31}k_{10})$ predominates for $E_1 < 0.2$ V. Thus in the first case

$$k_{\text{slow}}^{ap} \approx k_{32}\left(1 + \frac{1}{K_{30}}\right) \tag{10}$$

Since here $K_{30} \approx 90$, one has simply $k_{\text{slow}}^{ap} \approx k_{32}$, which accounts for the behavior of this function at high E_1. In the low E_1 region

$$k_{\text{slow}}^{ap} \approx K_{31}k_{10}\left(1 + \frac{1}{K_{30}}\right) = \frac{K_{30}}{K_{10}}k_{10}\left(1 + \frac{1}{K_{30}}\right) = k_{01}(1 + K_{30}) \tag{11}$$

Thus, $k_{\text{slow}}{}^{ap} \approx 90\ k_{01}$, accounting for the observed behavior in this region.

In the region where E_1 is close to or larger than E_0, the experimentally observed slow phase does not pertain to the one-electron configuration but rather to the two-electron one (unless some special procedure is devised). Indeed, in this case, one will generally have c_{556}, c_{559}, and P reduced in the dark-adapted state. Thus, following a flash, the transfer from c_{556} will be slowed because of the electron that has equilibrated during the fast phase between P and c_{559}. One may anticipate[24] that under such circumstances, the two-electron rate can be obtained by multiplying the one-electron expression by the fraction of oxidized c_{559} in equilibrium with P, i.e., (for a more complete discussion, see eqs S16−17 in Appendix B, Supporting Information)

$$k_{\text{slow}}{}^{ap\prime} \approx k_{\text{slow}}^{ap}\frac{K_{10}}{1 + K_{10}} \tag{12}$$

This expression was plotted in Figure 4c (open circles). It matches α_{2S} at high E_1 values and α_{1S} at low E_1 so that it can be used as a good approximation of k_{slow} throughout.

Considering the experimental data from the two strains of *B. viridis* (yellow symbols in Figure 4C), the kinetic analysis predicts that, in both cases $k_{\text{fast}} \approx k_{10}$ and $k_{\text{slow}} \approx k_{32}$. This prediction relies on the energetic pattern but depends little on the values assumed for the λ's. We took advantage of this to

adjust the reorganization energy λ_{10} so that $k_{10}(\lambda_{10})$ matches the experimental value of k_{fast} and similarly, λ_{32} was chosen so that $k_{32}(\lambda_{32})$ matches the experimental k_{slow}. This yields $\lambda_{10} \approx 0.500$ eV and $\lambda_{32} \approx 0.860$ eV. The kinetic behavior is little dependent on λ_{21}, and we set its value arbitrarily at $(\lambda_{10} + \lambda_{32})/2$. Chen et al.[20] had also noticed that the adjustment of the data required $\lambda_{10} < \lambda_{32}$. Their estimates were different from the present ones, however, because the correction of the energy landscape from the interactions between redox centers was not handled correctly.

The value of E_1 achieved in the R264K mutant of *B. viridis* is close to the transition where the rate limitation for the slow phase shifts from step *3* → *2* (eq 10) to step *1* → *0* (eq 11). As shown in the next section, some of the chimeric RCs studied in the present work are located deep within the second region. It may be noticed that the different rate limitation regimes should affect the apparent activation enthalpy E_{ac} (i.e., the slope of an Arrhenius plot) of the slow phase. When k_{32} is rate-limiting, the temperature dependence should be that predicted by ET theory for an uphill rate constant, which implies $E_{ac} > \Delta G$. For example, the activation energy predicted by Marcus' equation is $\approx (\lambda + \Delta G)^2/4\lambda$ (where ΔG is positive), which gives ~310 meV with the present values of ΔG_{32} (172 meV) and λ_{32} (860 meV). The quantum mechanical expression of Jortner also predicts $E_{ac} > \Delta G$, but the difference is less pronounced. Chen and co-workers[14] actually measured $E_{ac} \approx 220$ meV for the WT and R264K mutant of *B. viridis*. In the other regime, where step *1* → *0* is rate-limiting, equilibration is achieved in the upstream section of the chain, so that E_{ac} reflect essentially the height of the uphill barrier, i.e., ΔG_{32} (or ΔG_{31}, for the chimeric strains where $E_1 < E_2$).

Analysis of the Kinetic Data from Chimeric RCs. The same procedure as above was applied to construct Figure 5 based on the energy pattern of the chimeric RC family. We made the starting assumption that the distances and λ's used for *B. viridis* were essentially valid for the family of chimeric RCs. This view is supported by two pieces of evidence. First, the crystallographic structure of the R246K mutant RC of *B. viridis* was resolved by Chen et al.,[20] showing that the tetraheme structure was not significantly modified by this type of mutation. Second, the orientation of the g_z vector of heme c_{559} was determined in VC−F from EPR on oriented samples,[24] showing that the chimeric construct presents a very similar pattern to that of the *B. viridis* WT strains. Nevertheless, as shown below, the agreement between the kinetic data from the chimeric family and theoretical predictions can be improved by slightly modifying some distance or λ parameters with respect to *B. viridis*.

The horizontal axis in Figure 5 is ΔG_{10} rather than E_1, because of the non unique relationship between both quantities (Table 2). The experimental datapoints were plotted at the values indicated in the Table 2 for option (†), subtracting 40 mV to account (conservatively) for the shift of E_0 inferred from the dynamic equilibria. The rate of the fast phase (pink diamonds) is slightly smaller than in the *B. viridis* strains (yellow diamonds) and to restore a good agreement with k_{fast}^{ap}(eq 6; pink curve) one may increase slightly λ_{10} (to 0.6 eV) or R_{10} (to 12.9 Å) with respect to the fit shown in Figure 4 for *B. viridis*. The latter option was adopted, as some modification of R_{10} is not unlikely in the chimeric constructs. This modification accounts for the downshift of the k_{10} and k_{01} curves, while the other *k*'s are close to those of Figure 4 (taking into account the shift due to the higher E_0 in the chimeras). The approximation function $k_{slow}^{ap}{}'$ of eq 12 is shown as the thick solid green line (again equivalent to the relevant eigenvalues of the kinetic matrix). In the low ΔG_{01} region it is close to 2 k_{01} as predicted from eq 11, with $K_{30} \approx 1$ (this is the estimate derived from dynamic equilibria). This accounts for the difference with respect to the corresponding curve for *B. viridis* (yellow), where $K_{30} \approx 90$. In the high ΔG region, the approximation curve (solid green line) is systematically above the datapoints, suggesting that the k_{32} rate is smaller than estimated. We note that this may be remedied (dashed green curve) by assuming an increased R_{32} (e.g., from 7.89 to 8.9 Å) or an increased λ_{32} (e.g., 1.1 eV instead of 0.86 eV), although there is no obvious reason for structural changes in this region.

It is interesting to note that in the low ΔG region, the ratio between the fast and slow phase rates is determined by the energetic pattern (equilibrium constants), irrespective of any theoretical expression for the ET rate (i.e., eq 2), provided that the approximation formula (eq 11) applies. Indeed, one has then

$$\frac{k_{fast}}{k_{slow}} \approx \frac{k_{10}}{k_{01}(1 + K_{30})} = \frac{K_{10}}{1 + K_{30}} \qquad (13)$$

Then, considering the three lowest potential mutants for which the experimental ratio k_{fast}/k_{slow} is ~6000 (from Table 1), eq 13 predicts (with $K_{30} \approx 1$): $K_{10} \approx 12\,000$ or $\Delta G_{10} \approx -235$ meV. This is in good agreement with the ΔG_{10} values (−241 and −226 meV, obtained by implementing the 40 meV correction of E_0 to the values of Table 2 for the one electron case). In contrast, the other possible allocation of the E_m's between hemes c_{559} and c_{552} (see above) would make ΔG_{10} less exergonic by ~50 mV (~130 meV + Ψ_{21}), which gives a definitely poorer agreement. We emphasize that this argument based on eq 13 makes no use of the Moser-Dutton[30] approximation and relies only on the kinetic data (rates and dynamic equilibria).

Discussion

When the roller coaster arrangement of cofactors in the tetraheme became known, it was still unclear whether the low potential hemes were actual intermediates for electron transfer or should be considered as passive conductive regions for electron transfer between the high potential partners (see ref 33 for an early discussion). Support for the former view has accumulated ever since. Mathis and co-workers[20,26] pointed out that the observed kinetic rate was strongly favoring this option. Despite the low equilibrium constant for reducing c_{552} from c_{556}, the short distance between the two partners renders this event sufficiently frequent for allowing an acceptable overall rate for ET along this route. Direct transfer from c_{556} to c_{559}, on the other hand, would be much too slow because of the exponential dependence of ET rate on distance.[1,30] The data obtained on the R264K mutant of *B. viridis* were consistent with the interpretation that the uphill step (k_{32}) is responsible for rate limitation.[20] The present work provides a further demonstration of this picture, showing that the kinetic effects observed in mutants with modified cofactor potentials are in good agreement with predictions based on this kinetic model and on the dependence of rates on ΔG predicted by current ET theory.

The set of chimeric mutants examined in this work has allowed us to investigate the effect of modifying the midpoint

potential of a redox center, heme c_{559}, over a potential span of ~400 mV. Of interest is the fact that the explored range goes past the midpoint potentials of the upstream and downstream partners, thus introducing novel uphill steps. In particular, this provides useful information concerning the interaction energies between the redox centers. The comparison of the redox titration data of the "chimeric wild type" strain VC−F and of the native strains allowed to estimate the interaction $\Psi_{10} \approx 50$ meV between c_{559} and P. Similarly, the upward shift by ~70 mV of the E_m of c_{552} in mutants where c_{559} is more reducing than c_{552} yields an estimate of Ψ_{21}, which is in good agreement with the value obtained from electrostatic calculations. These interactions must be properly taken into account for assessing the effective energy landscape from redox titrations. In particular, this weakens quite significantly the uphill character of the $c_{556} \rightarrow c_{552}$ step. A particular feature of the chimeric RC is that the high potential hemes and P have nearby midpoint potentials, due to the ~100 mV higher E_m of P in *B. viridis* with respect to *R. gelatinosus*. This sensitive situation with respect to ET equilibria provided evidence that the midpoint potential of P in the ms time range after charge separation is at least 40 mV lower than indicated by redox titrations.

We developed a complete analytical treatment for the kinetics in a 4-component ET chain. This allowed us to establish the validity of approximation formulas for the fast and slow phases of P^+ reduction, thereby gaining a more intuitive grasp on the determining factors. These rates bear on important functional features: the fast one determines the lifetime of P^+ after the photochemical act and competes with recombination; the slow phase indicates the maximal rate that this section of the chain is able to sustain in a steady-state regime. The analysis shows that in *B. viridis* WT, the rate-limiting step is the uphill transfer from c_{556} to c_{552} (k_{32}). When decreasing the midpoint potential of heme c_{559}, the rate-limitation becomes eventually located on the final step, $c_{559} \rightarrow P$, although the rate constant on this step, k_{10}, increases as the reaction becomes more exergonic. The prevailing effect in this regime is the decrease of the equilibrium constant for the (now uphill) overall transfer from c_{556} to c_{559}. The location of the transition between both rate-limitation regimes, when modifying the energy profile, is of course highly dependent on the distances between redox centers. A critical parameter at each link in an ET chain is the ratio of forward over backward rate constants out of a redox center (e.g., k_{21}/k_{23} for redox center *2*), which enters the steady-state rate constant as a "transmission coefficient", e.g., $1/(1+ k_{21}/k_{23})$ (see eq S11 in Appendix B, Supporting Information). The arrangement in *B. viridis* WT is such that all transmission coefficients are close to 1. Concerning redox center *1* (c_{559}), the inequality $k_{10} > k_{12}$ is essentially achieved by the energy profile, because k_{10} is downhill and k_{12} uphill. The effect is sufficiently large to overcome the opposite role played by distances ($R_{10} > R_{21}$). On the other hand, because of the relatively weak dependence of downhill rate constants vs ΔG, the energy profile by itself (i.e., the fact that $E_1 > E_3$) would not suffice to make $k_{21} \gg k_{23}$, whereas this is achieved by having R_{21} slightly smaller than R_{32}. The same considerations apply also for heme c_{554} with $R \approx 7.1$ Å on the downstream side and 7.8 Å on the upstream side.[7,8] In the chimeric strains, however, the transmission coefficient of c_{559} is <1 ($k_{10} < k_{12}$, because of the more positive E_0) and the rate is always smaller than k_{32}. Formulated in a general way, this analysis suggests that when an uphill intermediate is present (in natural ET chains), it should be located closer to its downstream partner than to its upstream partner.

One conclusion from the present work and from ref 20 is that the kinetic performance of this section of the chain is rather robust, meaning that relatively large changes of the midpoint potentials may occur with little consequence (e.g. the 110 mV change of E_1 in the R264K mutant of *B. viridis*, or the 100 mV shift of E_0 in VC−F compared to *B. viridis*). In this particular section, the $c_{556} \rightarrow c_{552}$ transfer is the rate-limiting step (in the WT), whereas on a broader scale it is the other uphill step from (bound) cytochrome c_2 to the c_{554} heme.[15] The question remains unsolved, however, of the nature of the selection pressure that conserves the roller coaster arrangement in some ET chains. The fact that such arrangements can accomplish perfectly well their kinetic function[1,34] does not explain why this type of design has been so strictly conserved over distantly related organisms. For instance, using the kinetic tools described in this paper, one sees that a drift of the c_{552} toward a higher potential can only improve the kinetic performance. There is probably no advantage in achieving a still faster limiting rate, but the question is, why should such a drift be counter-selected? The reason may not be primarily kinetic. It has been suggested[16] that it could be important to insert low potential hemes, which remain essentially oxidized under normal physiological conditions, to separate spatially the high potential hemes. This avoids electrostatic interactions that might render the energy profile of the chain too variable, depending on the number of charges present.

Acknowledgment. This work was supported in part by grants from the Ministry of Education, Science and Culture of Japan to K.V.P.N. Support by the CNRS and CEA is acknowledged.

Supporting Information Available: The expressions of the evolution matrixes **M** are indicated in Appendix A. Appendix B gives a derivation and discussion of the approximate formula for the rate of the slow phase. This material is available free of charge via the Internet at http://pubs.acs.org.

JA058131T

(34) Page, C. C.; Moser, C. C.; Dutton, P. L. *Curr. Opin. Chem. Biol.* **2003**, *7*, 551−6.